enhanced) in water vapor. The distribution of water ice throughout the solar nebula may have varied with heliocentric distance and with time (*12*), producing environments with varying rock/water ratios. The existence of extensively hydrated FGRs contained within aqueously altered meteorites implies that the formation of chondrules and eventually meteorite parent bodies may have extended into the region where Jupiter eventually formed.

References and Notes

1. K. Metzler, A. Bischoff, D. Stoffler, *Geochim. Cosmochim. Acta* **56**, 2873 (1992).
2. D. S. Lauretta, X. Hua, P. R. Buseck, *Geochim. Cosmochim. Acta* **64**, 3263 (2000).
3. M. R. Lee, *Meteoritics* **33**, 53 (1993).
4. R. G. Prinn, B. Fegley Jr., *Ann. Rev. Earth Planet. Sci.*, **15**, 171 (1987).
5. B. Fegley Jr., R. G. Prinn, *The Formation and Evolution of Planetary Systems* (Cambridge Univ. Press, Cambridge, 1989), p. 171.
6. H. C. Connolly Jr., S. G. Love, *Science* **280**, 62 (1998).
7. A. Ida, T. Nakamoto, H. Susa, *Icarus* **153**, 430 (2001).
8. S. J. Desch, H. C. Connolly Jr., *Meteorit. Planet. Sci.* **37**, 183 (2002).
9. F. J. Ciesla, L. L. Hood, *Icarus* **158**, 281 (2002).
10. K. D. Supulver, D. N. C. Lin, *Icarus* **146**, 525 (2000).
11. D. J. Stevenson, J. I. Lunine, *Icarus* **75**, 146 (1988).
12. K. E. Cyr, W. D. Sears, J. I. Lunine, *Icarus* **135**, 537 (1998).
13. Y. Amelin, A. N. Krot, I. D. Hutcheon, A. A. Ulyanov, *Science* **297**, 1678 (2002).
14. S. J. Weidenschilling, *Meteorites and the Early Solar System* (Univ. of Arizona Press, Tucson, AZ, 1988), p. 348. The time scale for settling to the midplane for 1-mm ice particles for conditions considered here is ~104 years, much less than the time periods considered.
15. J. N. Cuzzi, R. C. Hogan, J. M. Paque, A. R. Dobrovolskis, *Astrophys. J.* **546**, 496 (2001).
16. Gravitational settling would create a roughly uniform concentration of particles at some given distance from the sun, whereas models of turbulent concentration predict a variety of concentrations in different regions throughout the nebula. Gravitational settling will lead to concentrations of solids that are a few hundred times greater than that of the canonical solar nebula (*14*). Turbulent concentration models predict that concentrations orders of magnitude larger are possible (*15*). It should be pointed out that neither of these concentration mechanisms have been investigated by including diffusive redistribution of a condensable species like water vapor. Also, our model does not require that an entire region of the nebula be enhanced with water ice, but rather only relatively small regions (~ a few hundred km). Significant enhancements of solids such as water ice certainly existed during the early planetesimal building stage (*14*).
17. R. H. Hewins, H. C. Connolly Jr., *Chondrules and the Protoplanetary Disk* (Cambridge Univ. Press, Cambridge, 1996), p. 197.
18. H. C. Connolly Jr., B. D. Jones, R. H. Hewins, *Geochim. Cosmochim. Acta*, **62**, 2725 (1998).
19. W. W. Wegner, W. G. Ernst, *Am. J. Sci. Ser. A* **283**, 151 (1983).
20. D. W. G. Sears, G. D. Akridge, *Meteorit. Planet. Sci.* **33**, 1157 (1998).
21. Such conditions could be reached in a variety of ways. In addition to the enhancement mechanisms mentioned above, radial drift of ice particles from the snow line may have enhanced water ice in the solar nebula from 3 to 5 AU (*12*). If the processing described in this report occured in a warmer region of the nebula, the time that the system would take to cool through the temperature range of interest would be longer than that for the case considered here.
22. Thermodynamic equilibrium calculations were performed with the use of the equilibrium module in the HSC Chemistry v5.0 software package, produced by Outokumpu Research Oy (Pori, Finland). This module calculates multicomponent equilibrium compositions in heterogeneous systems with the use of a database of over 15,000 compounds and a Gibbs energy minimization equilibrium solver. The system is composed of H, He, C, N, O, Mg, Si, S, and Fe. The abundances of all elements except H and O are set at solar system abundances (*23*). The abundances of H and O are enhanced consistent with an ice abundance of 700× solar. The species considered in the calculations included 127 different gaseous molecules as well as Fe metal, forsterite, fayalite, enstatite, ferrosilite, troilite, chrysotile, greenalite, wustite, magnetite, hematite, brucite, Fe(II) hydroxide, Fe(III) hydroxide, graphite, SiC, cohenite, siderite, magnesite, sinoite, and water ice. Thermodynamic data for cronstedtite, the most abundant Fe-bearing phase in phyllosilicate-rich accretionary rims, are not available. However, a thermodynamic model for greenalite, a mineral similar in composition and structure to cronstedtite, was recently developed (*24*), and we use this phase to represent Fe-bearing phyllosilicate material. Thermodynamic data for all other species are included in the software database.
23. K. Lodders, B. Fegley, *The Planetary Scientist's Companion*, 80 (Oxford Univ. Press, New York, 1998), p. 80.
24. M. G. Rasmussen, B. W. Evans, S. M. Kuehner, *Can. Mineral.* **36**, 147 (1998).
25. H. C. Connolly Jr. *et al.*, *Nature* **371**, 136 (1994).
26. D. S. Lauretta, P. R. Buseck, T. J. Zega, *Geochim. Cosmochim. Acta* **65**, 1337 (2001).
27. This reaction time was calculated as the amount of time it would take for an iron grain to react with water vapor to form magnetite using the data from (*4*). Magnetite becomes stable in a system of just H, He, C, N, O, S, and Fe at ~1500 K. Thus, if an iron grain is expelled from the chondrule melt, it will start to form magnetite as the system cooled below this temperature. To be conservative, the time scale here was calculated at 1000 K. The reaction would be much more rapid at the higher temperatures, though the system may cool rapidly at these temperatures.
28. R. E. Grimm, H. Y. McSween Jr., *Icarus* **82**, 244 (1989).
29. B. A. Cohen, R. F. Coker, *Icarus* **145**, 369 (2000).
30. A. Bischoff, *Meteorit. Planet. Sci.* **33**, 1133 (1998).

31. The authors thank H. Connolly, J. Nuth, and two anonymous reviewers for useful discussions and comments and M. Pasek for help in carrying out the equilibrium calculations. Supported by a grant from the NASA Origins program. This is Hawaii Institute of Geophysics and Planetology publication no. 1253 and School of Ocean and Earth Science Technology publication no. 6076.

15 October 2002; accepted 13 December 2002

Robust Normal Mode Constraints on Inner-Core Anisotropy from Model Space Search

Caroline Beghein,* Jeannot Trampert

A technique for searching full model space that was applied to measurements of anomalously split normal modes showed a robust pattern of *P*-wave and *S*-wave anisotropy in the inner core. The parameter describing *P*-wave anisotropy changes sign around a radius of 400 kilometers, whereas *S*-wave anisotropy is small in the upper two-thirds of the inner core and becomes negative at greater depths. Our results agree with observed travel-time anomalies of rays traveling at epicentral distances varying from 150° to 180°. The models may be explained by progressively tilted hexagonal close-packed iron in the upper half of the inner core and could suggest a different iron phase in the center.

The concept of inner-core anisotropy is generally accepted as an explanation for the directional dependence of PKIKP travel times and the anomalous splitting of core-sensitive free oscillations (*1*, *2*). Several models have tried to explain both kinds of data, but amplitude and depth dependence of the anisotropy are still a matter of debate (*1*–*7*). In particular, models derived from the inversion of normal mode data cannot explain the large travel-time anomalies observed for body waves traveling at high epicentral distances (*8*–*10*). Even joint inversions of normal mode and travel-time data fail to reconcile all observations (*4*, *5*, *11*). Outer-core structure was even suggested to explain all existing data but could not account for the strong splitting of modes highly sensitive to inner-core structure (*6*). The inner core is believed to be mainly composed of solid iron, with some unknown light elements (*12*–*16*). Although the stable phase of iron at inner-core conditions is not known, mineralogical studies tend to favor a hexagonal close-packed (h.c.p.) structure. Nevertheless, the possibility of another stable phase is not excluded, especially in the presence of lighter elements (*15*). Estimates of the elastic properties of h.c.p. iron at high pressure and temperature (*17*) suggest that the basal plane of one-third of the crystals would have to be aligned with Earth's spin axis to match travel-time observations.

The inner core is generally modeled as a cylindrical medium with a symmetry axis parallel to Earth's rotation axis (*1*, *2*). In that case, normal mode theory (*18*) shows that zonal structure coefficients at degrees two and four are linearly related to three parameters that describe seismic anisotropy:

Faculty of Earth Sciences, Utrecht University, Post Office Box 80021, 3508 TA Utrecht, Netherlands.

*To whom correspondence should be addressed. E-mail: beghein@geo.uu.nl

$$c_{s0} = \int_0^{R_{icb}} [\alpha(r) K_s^{\alpha} + \beta(r) K_s^{\beta} + \gamma(r) K_s^{\gamma}] dr \quad (1)$$

where s is the spherical harmonic degree, r is the radius, R_{icb} stands for the radius of the inner core, and c_{s0} is the measured structure coefficient at degree s and order zero of a given mode. α, β, and γ are the three anisotropic parameters describing *P*-wave anisotropy, *S*-wave anisotropy, and the anisotropy of waves that do not travel along the vertical or horizontal directions, respectively. They are related to the well-known Love coefficients A, C, N, L, and F (*19*) as follows: $\alpha = (C - A)/A_0$, $\beta = (N - L)/A_0$, and $\gamma = (A - 2N - F)/A_0$, with A_0 the value of elastic parameter A at the center of Earth. C and L are related to the speed of *P* and *S* waves traveling parallel to Earth's rotation axis; A and N, to waves traveling perpendicular to Earth's rotation axis. K_s^{α}, K_s^{β}, and K_s^{γ} are the sensitivity kernels of a given mode to Earth's structure. The three model parameters were expanded on a series of five cubic spline functions with knots equally spaced through the inner core. The anisotropic models are found by inverting or solving Eq. 1 for the spline coefficients.

We established that discrepancies among existing seismological models of inner-core anisotropy are mainly due to regularization, which stabilizes the inverse problem defined by Eq. 1. Regularization or damping is needed to force a solution in the presence of nonuniqueness because of bad model sampling or contradictions in the data. Because normal mode data are sensitive not only to the core but also to the overlying mantle, another possible source of uncertainty is the three-dimensional mantle model used to correct the measurements. From inversions by singular value decomposition (*20*), we found that regularization and data quality had a substantial influence on the final model, whereas the chosen mantle model was less crucial (Fig. 1). We used different levels of damping and two sets of data, consisting of zonal degree two and degree four structure coefficients and their error estimates (*21*). The first data set consisted of older measurements (*22*, *23*), whereas the second data set resulted from the most recent splitting measurements that followed the great Bolivia and Kuril Islands earthquakes in 1994 (*24*–*26*). All data were corrected with the crustal model CRUST5.1 (*27*). Various mantle models (*28*–*35*) were tested (*21*). For all data sets, we observed that the choice of the mantle model does not have a profound effect on the solution: It affects the amplitude of the anisotropy but not the depth pattern. The regularization, however, changes the models significantly. In general, a higher damping pushes the anisotropic signal into shallower parts of the inner core. We further observed that inversions of the older measurements produced models with the maximum of *P*-wave anisotropy situated at the top of the inner core, whereas including more recent data shifts this maximum to greater depths. All models obtained by damped inversions showed small amplitudes in the innermost inner core because of the nature of the sensitivity kernels. Therefore, they cannot predict the large travel-time anomalies observed for waves traveling in a north-south direction (*8*–*10*).

The strong dependence of the obtained anisotropic model on damping indicates the presence of a large model null space (the part of the model space not constrained by the data). In addition, inversions do not provide realistic posterior model uncertainties because of a complete trade-off between variance and resolution (*36*). To obtain all possible models of inner-core anisot-

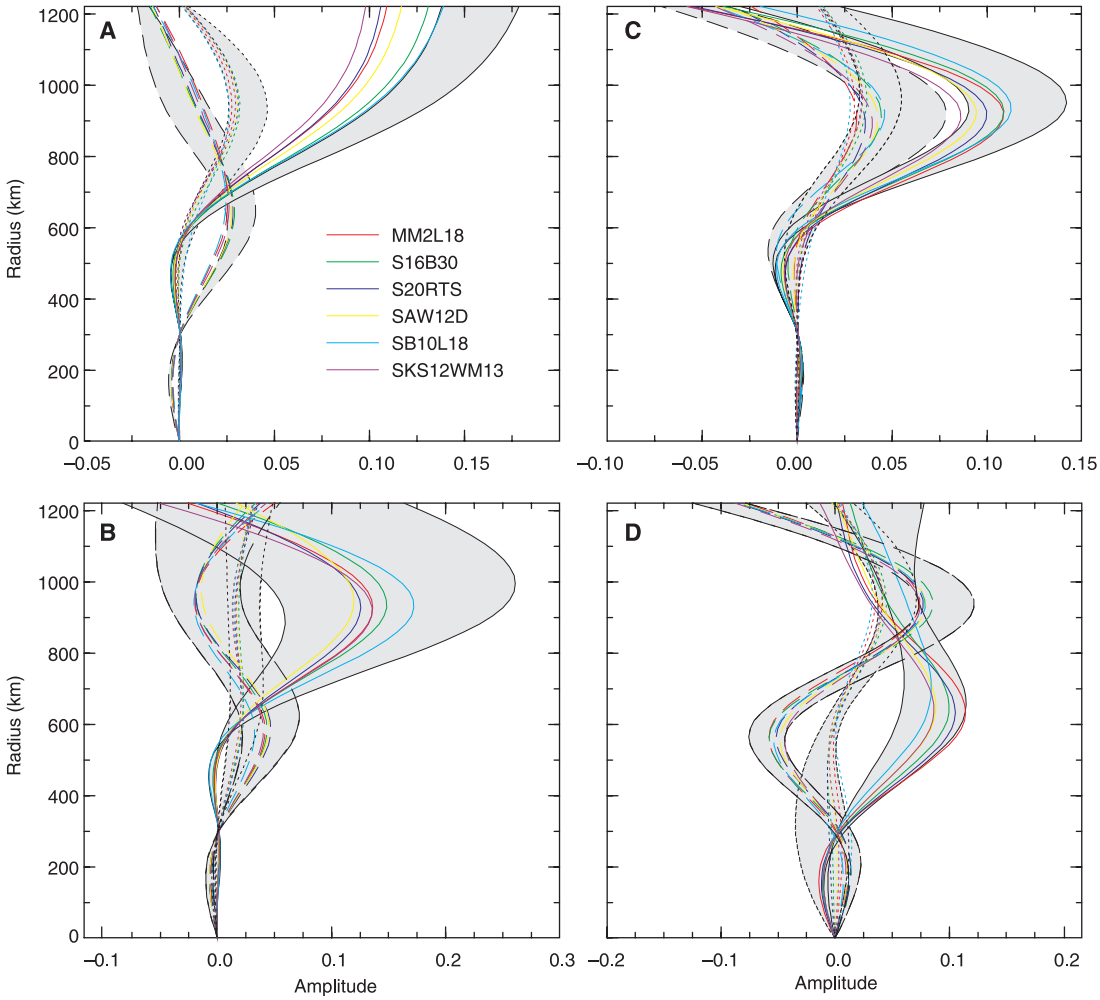

Fig. 1. Models resulting from the inversion of older (**A** and **B**) and recent (**C** and **D**) data are shown. Two levels of damping were applied. (A) and (C) correspond to highly damped models; (B) and (D) are models for which the constraint of the damping was lower. The solid lines represent *P*-wave anisotropy; the dotted lines, *S*-wave anisotropy; and the dashed lines, parameter γ. Different mantle models (*21*) were used to correct the data, yielding the inner-core models in color and in the gray areas.

ropy compatible with free oscillation data, we employed a forward modeling approach, the neighborhood algorithm (NA) (*37*, *38*). With such a method, the entire model space is explored, no regularization is introduced, and the model parameter uncertainties and correlations can be obtained. The NA has recently been made available and successfully used in small-size tomographic studies (*29*, *30*, *39*). We used the NA to survey the entire model space and found the ensemble of inner-core models that fit the selected splitting data (*21*). Because the free oscillations were strongly excited by the Bolivia and Kuril Islands earthquakes of 1994, we applied the NA to the most recent anomalous splitting measurements only (*21*). The resulting models of inner-core anisotropy fit the data with a χ misfit lower than 3 regardless of the mantle correction applied (*21*). The results present several robust characteristics (Fig. 2). First, for most models, α is positive in the upper half of the inner core (r = 500 to 1200 km), with amplitude increasing down to the middle of the inner core and becoming negative at greater depths. The fast direction for *P* waves is thus along the rotational axis in the middle of the inner core but becomes parallel to the equatorial plane at greater depths. Second, β is small and slightly positive in the upper two-thirds of the inner core and becomes negative in the lower 400 km of the core. Thus, shear waves sampling the innermost inner core are expected to move faster along the rotational axis than along the equatorial plane. Third, γ is negative at the inner-core boundary and undergoes two successive changes of sign around r = 1100 km and r = 600 km. All these features are robust and independent of the mantle correction (*21*). The most interesting finding is that many models show an anisotropic signal at large depths, as opposed to inversion results where the damping drives the innermost core anisotropy to zero. There are some features that are not as well constrained: α and γ have much larger errors at the very bottom of the inner core, and their signs are not robust. Their values at large depths are not independently constrained by our data, as can be seen on the correlation matrix (Fig. 3).

To test the compatibility of this family of inner-core models with observed differential travel-time anomalies, we generated random samples according to the posterior probability density functions associated with each model parameter (*21*). *P*-wave velocity anomalies associated with inner-core anisotropy are given by (*1*):

$$\frac{\delta v}{v_{eq}} = (2\beta - \gamma)\cos^2\xi + \left(\frac{1}{2}\alpha - 2\beta + \gamma\right)\cos^4\xi \qquad (2)$$

where ξ is the angle between the ray and Earth's rotation axis and v_{eq} is the equatorial velocity. Predictions of differential travel-time anomalies are computed for waves traveling at about 153° epicentral distance, which sample the upper 290 km of the inner core, and for rays traveling at 170° epicentral distance, which turn at a radius of about 350 km (Fig. 4). We also computed predictions in the epicentral range from 168° to 180°. All models produced, irrespective of the mantle correction, are compatible with the observed travel-time anomalies of rays sampling the upper quarter of the core, and most of them predict anomalies between 4 and 6 s for rays traveling in a north-south direction, which confirms the estimates made from mantle-corrected travel-time data (*10*).

Our results are robust and independent of the mantle model used to correct the data. The full model space search identified previously unknown solutions from damped inversions and produced models with the use of normal mode data alone that agree with the observed differential travel-time anomalies of rays traveling through the inner core at epicentral distances varying between 150° and 180°. More detailed than a division between bulk and innermost inner core (*11*), a simple model of radially varying cylindrical anisotropy is sufficient to explain splitting and travel-time data without needing outer-core structure (*6*). A comparison with the latest determination of the elasticity of h.c.p. iron at inner-core conditions (*17*) shows that some of our models can be explained by progressively tilted h.c.p. iron in the upper half of the inner core, with their symmetry axes oriented at 45° from Earth's rotation axis at r = 900 km and at 90° in the middle of the inner core. In the deepest inner core (r = 0 to 400 km), none of our models is compatible with published data of h.c.p. iron. This result might suggest the presence of an-

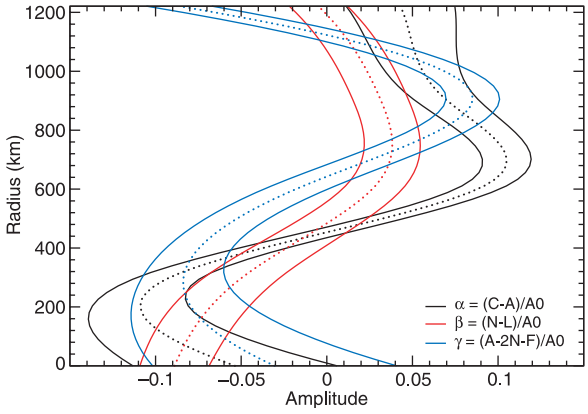

Fig. 2. Models resulting from the application of the NA using mantle (*29*). The thin dotted line represents the mean model, and the thick surrounding lines correspond to two standard deviations taken from the posterior probability density functions obtained from the NA.

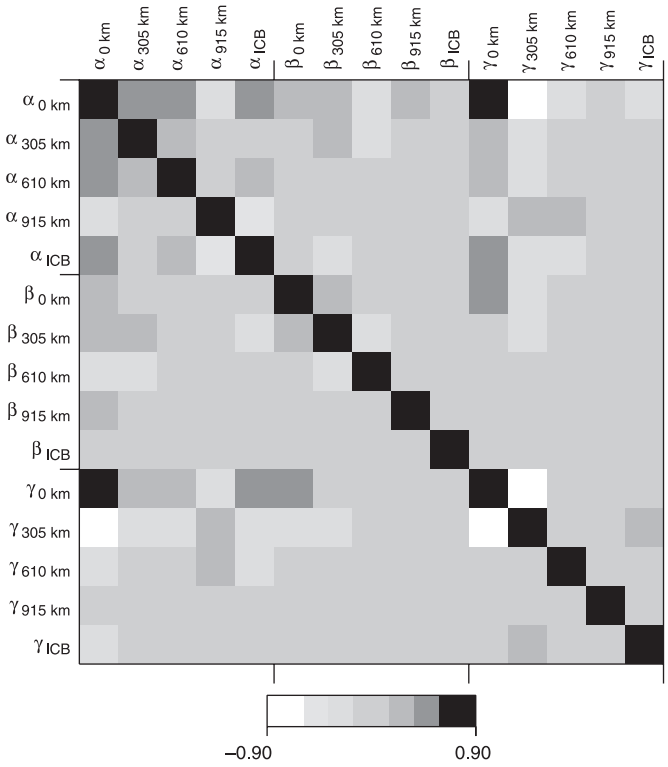

Fig. 3. Correlation matrix corresponding to the family of models in Fig. 2. Indices correspond to the radii of the different spline knots. The off-diagonal elements in the matrix describe how the data link the different model parameters together. ICB indicates the inner-core boundary.

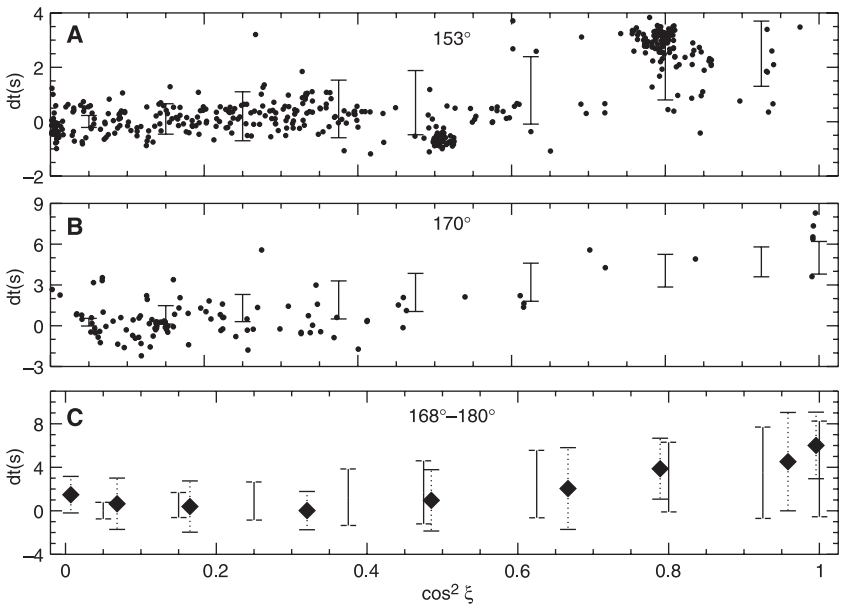

Fig. 4. Predictions of differential travel-time anomalies PKP(BC)-PKP(DF) at the epicentral distance of 153° (**A**) and PKP(AB)-PKP(DF) at the epicentral distance of 170° (**B**) and in the range of 168° to 180° (**C**). The dots in (A) and (B) are data points for waves traveling in the epicentral distance range from 147° to 153° and from 167° to 173°, respectively (*7*). The diamonds in (C) are binned AB-DF data between 168° and 180°, with two standard deviations (*10*). These estimations are on the basis of a random prediction from the family of models shown in Fig. 2. The solid vertical lines represent two standard deviations of our predictions (*21*).

other phase from these depths. Such a phase of iron could indeed be stable in the presence of impurities (*15*).

References and Notes

1. A. Morelli, A. Dziewonski, J. Woodhouse, *Geophys. Res. Lett.* **13**, 1545 (1986).
2. J. Woodhouse, D. Giardini, X.-D. Li, *Geophys. Res. Lett.* **13**, 1549 (1986).
3. J. Tromp, *Nature* **366**, 678 (1993).
4. _____, *GSA Today* **5**, 137 (1995).
5. J. Durek, B. Romanowicz, *Geophys. J. Int.* **139**, 599 (1999).
6. B. Romanowicz, L. Bréger, *J. Geophys. Res.* **105**, 21559 (2000).
7. K. Creager, *Geophys. Monogr. Am. Geophys. Union 117* (American Geophysical Union, Washington, DC, 2000), pp. 89–114.
8. W.-J. Su, R. Woodward, A. Dziewonski, *J. Geophys. Res.* **100**, 9831 (1995).
9. X. Song, *J. Geophys. Res.* **101**, 16089 (1996).
10. X. Sun, X. Song, *Earth Planet. Sci. Lett.* **199**, 429 (2002).
11. M. Ishii, A. Dziewonski, *Proc. Natl. Acad. Sci. U.S.A.* **99**, 14026 (2002).
12. F. Birch, *J. Geophys. Res.* **69**, 4377 (1964).
13. L. Stixrude, E. Wasserman, R. Cohen, *J. Geophys. Res.* **102**, 24729 (1997).
14. H. K. Mao *et al.*, *Science* **292**, 914 (2001).
15. J.-F. Lin, D. L. Heinz, A. J. Campbell, J. M. Devine, G. Shen, *Science* **295**, 313 (2002).
16. C. Gessman, B. Wood, *Earth Planet. Sci. Lett.* **200**, 63 (2002).
17. G. Steinle-Neumann, L. Stixrude, R. Cohen, O. Gülseren, *Nature* **413**, 57 (2001).
18. J. Tromp, *Geophys. J. Int.* **121**, 963 (1995).
19. A. Love, *A Treatise on the Mathematical Theory of Elasticity* (Cambridge Univ. Press, Cambridge, 1927).
20. M. Matsu'ura, N. Hirata, *J. Phys. Earth* **30**, 451 (1982).
21. Materials and methods are available as supporting material on *Science* Online.
22. M. Ritzwoller, G. Masters, F. Gilbert, *J. Geophys. Res.* **93**, 6369 (1988).
23. R. Widmer, G. Masters, F. Gilbert, *Geophys. J. Int.* **111**, 559 (1992).
24. J. Tromp, E. Zanzerkia, *Geophys. Res. Lett.* **22**, 2297 (1995).
25. X. He, J. Tromp, *J. Geophys. Res.* **101**, 20053 (1996).
26. J. Resovsky, M. Ritzwoller, *J. Geophys. Res.* **103**, 783 (1998).
27. W. Mooney, G. Laske, G. Masters, *J. Geophys. Res.* **103**, 727 (1998).
28. J. Resovsky, M. Ritzwoller, *J. Geophys. Res.* **104**, 993 (1999).
29. _____, J. Trampert, in preparation.
30. C. Beghein, J. Resovsky, J. Trampert, *Geophys. J. Int.* **149**, 646 (2002).
31. G. Masters, S. Johnson, G. Laske, H. Bolton, *Philos. Trans. R. Soc. London Ser. A* **354**, 1385 (1996).
32. J. Ritsema, H.-J. van Heijst, J. H. Woodhouse, *Science* **286**, 1925 (1999).
33. X. Li, B. Romanovwicz, *J. Geophys. Res.* **101**, 22245 (1996).
34. G. Masters, G. Laske, H. Bolton, A. Dziewonski, *Geophys. Monogr. Am. Geophys. Union 117* (American Geophysical Union, Washington, DC, 2000), pp. 63–87.
35. W.-J. Su, R. Woodward, A. Dziewonski, *J. Geophys. Res.* **99**, 6945 (1994).
36. G. Backus, F. Gilbert, *Philos. Trans. R. Soc. London Ser. A* **266**, 123 (1970).
37. M. Sambridge, *Geophys. J. Int.* **138**, 479 (1999).
38. _____, *Geophys. J. Int.* **138**, 727 (1999).
39. J. Resovsky, J. Trampert, *Geophys. J. Int.* **150**, 665 (2002).

40. M. Sambridge generously provided the codes of the NA. We wish to thank K. C. Creager, who provided the PKP(BC)-PKP(DF) and PKP(AB)-PKP(DF) data and the code giving travel-time anomalies as a function of the ray angle; X. Song, who sent us the differential travel-time data for the epicentral distance range of 168° to 180°; H. Paulssen for the numerous discussions concerning body waves and for computing the reference travel times for *P* waves inside the inner core; J. Resovsky for advice on the normal mode data; M. Ishii for a discussion concerning her inner-core work; and all the people who made their normal mode measurements and mantle models available in various publications.

Supporting Online Material

www.sciencemag.org/cgi/content/full/299/5606/552/DC1

Materials and Methods

5 September 2002; accepted 2 December 2002

An Evolutionary Advantage of Haploidy in Large Yeast Populations

Clifford Zeyl,* Thomas Vanderford,† Michele Carter‡

Although seed plants and multicellular animals are predominantly diploid, the prominence of diploidy varies greatly among eukaryote life cycles, and no general evolutionary advantage of diploidy has been demonstrated. By doubling the copy number of each gene, diploidy may increase the rate at which adaptive mutations are produced. However, models suggest that this does not necessarily accelerate adaptation by diploid populations. We tested model predictions regarding rates of adaptation using asexual yeast populations. Adaptive mutations were on average partially recessive. As predicted, diploidy slowed adaptation by large populations but not by small populations.

The evolutionary origins of diploidy, sex, and recombination, and their subsequent long-term effects, are often intertwined, both in evolutionary theory and in nature (*1–3*). The masking of recessive deleterious mutations (*4–7*) and the more frequent production of adaptive mutations (*8–10*) have both been hypothesized as evolutionary advantages of diploidy. We focused on the rates of adaptation in haploid and diploid yeast populations. In asexual populations, adaptation is typically thought to occur in a series of selective sweeps, each composed of two phases: a waiting period, representing the number of generations before the occurrence of the next adaptive mutation that escapes loss by genet-